communications
earth & environment

ARTICLE

https://doi.org/10.1038/s43247-022-00446-1 OPEN

Paleozoic ocean plate stratigraphy unraveled by calcite U-Pb dating of basalt and biostratigraphy

Goran Andjić[1,3]✉, Renjie Zhou[1]✉, David M. Buchs[2], Jonathan C. Aitchison[1] & Jianxin Zhao[1]

Oceanic mafic volcanic rocks preserve unique information regarding the nature and evolution of tectonic plates. However, constraining their age is commonly challenging because of their lack of datable minerals and high degrees of alteration. We present in situ laser ablation–inductively coupled plasma–mass spectrometry U-Pb dating of calcite phases in altered basalts in a Paleozoic subduction complex (eastern Australia). Calcite enclosed in amygdules and filled in fractures yielded two distinctive ages with contrasting geochemical signatures. These results, combined with new biostratigraphic and whole-rock geochemical data, suggest that oceanic islands formed in the Panthalassa Ocean at about 365 million years ago, accreted to eastern Gondwana at about 330 million years ago, and underwent brittle deformation at about 305 million years ago. Calcite U-Pb geochronology is valuable to help constrain minimum formation ages of volcanic rocks and their deformation history, ultimately improving ability to unravel the geological record of accretionary complexes, and more generally ancient underwater volcanic systems.

[1] School of Earth and Environmental Sciences, The University of Queensland, St Lucia, QLD 4072, Australia. [2] School of Earth and Environmental Sciences, Cardiff University, Cardiff, UK. [3] Present address: Department of Earth Sciences, Utrecht University, 3584 CB Utrecht, The Netherlands. ✉email: g.andjic@uu.nl; renjie.zhou@uq.edu.au

Remnants of ocean plate stratigraphy (OPS) in accretionary complexes preserve parts of the history of the oceanic crust from its formation at a mid-ocean ridge to its arrival at a trench, recording the evolution of oceanic plates and volcanic edifices that have been partly or entirely lost to subduction[1–5]. Circum-Pacific accretionary complexes contain a wide array of dismembered oceanic crust remnants from mid-ocean ridges, to intraplate and back-arc seamounts, oceanic plateaus, oceanic islands, and arcs[6–12]. Determining ages of formation and accretion of these remnants is critical to unraveling their origin and geological history. Biostratigraphic data from sedimentary rocks have been widely used to provide age constraints on accreted volcanic rocks and the formation of subduction complexes[13–17]. However, the age difference between the igneous substrate and the youngest sediments of a single volcanic edifice entering the subduction zone may reach up to 150 mega-year (Myr)[18,19], obscuring the geological meaning of biostratigraphic data in dismembered sequences. Directly dating the formation of accreted igneous rocks would resolve important research questions associated with OPS, but these rocks are generally mafic and may lack datable minerals or are too severely altered to be dated with common geochronological techniques[20–25].

Here we test whether U-Pb geochronology is a valid method to estimating the minimum formation age of altered volcanic rocks preserved in structurally complex settings. We explore the potential of U-Pb dating of calcite-filled amygdules in constraining ages of altered basalts in accretionary complexes by studying a selection of accreted volcanic remnants in a large, yet poorly studied late Paleozoic accretionary complex in the New England Orogen (eastern Australia), where existing age constraints were established by biostratigraphy on a selection of lithologies. New calcite in situ U-Pb geochronologic and geochemical, whole-rock geochemical, and radiolarian biostratigraphic data from a rock association typical of seamount OPS are provided, which constrain the ages of formation and accretion of oceanic islands within ca. ±20 mega-annum (Ma) precision, revealing both consistency and complementarity of information between the igneous and sedimentary components of dismembered OPS.

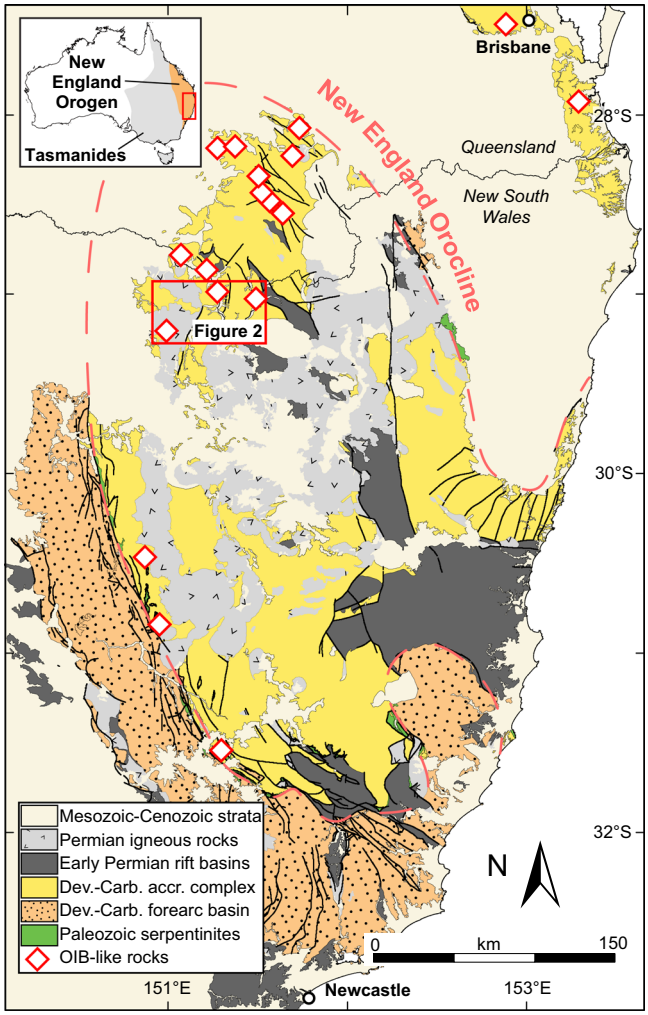

Fig. 1 Geological map of the southern New England Orogen (modified from ref. [49]). OIB-like rocks from refs. [34,35]. Accr. Accretionary, Dev.-Carb. Devonian-Carboniferous, OIB Ocean island basalt.

Geological setting. We studied the accretionary complex represented by the Carboniferous Texas Beds in the southern segment of the New England Orogen, which is the youngest belt of a collage of Paleozoic subduction-related orogens occupying the eastern third of the Australian continent[26–28] (Fig. 1). To the south, the complex occurs in association with a forearc basin (Tamworth Belt), whereas the associated magmatic arc is possibly concealed further west[29,30]. Early Permian granitoids, together with Devonian to early Permian forearc sedimentary rocks, outline the curvature of the New England Orocline, which is thought to have formed during the early to middle Permian (ca. 290–260 Ma)[30,31], after formation of the studied accretionary complex.

The accretionary complex was subject to low grade metamorphism and folding[32]. Altered ocean island basalt (OIB)-like rocks, cherts and shallow-marine carbonates are embedded throughout the complex[33–35] (Fig. 1). While igneous rocks remain undated, sedimentary rocks of intra-oceanic origins provide Ordovician to Carboniferous ages based on corals, radiolarians, and conodonts[33–35]. In our study area (Fig. 2), previous age constraints on the Texas Beds stem from red radiolarian cherts and massive shallow-marine carbonates. A radiolarian chert from Bonshaw yielded a late Visean–late Serpukhovian age (ca. 336–325 Ma)[33], whereas corals from massive carbonates in Ashford and Riverton yielded Visean ages (ca. 347–331 Ma)[34,35]. Although these rock associations are considered to represent remnants of oceanic islands based on existing biostratigraphic, geochemical and lithological data[34,35], their original relationship was obscured by tectonic dismemberment, possibly during accretion and/or gravitational collapse of islands arriving at the subduction zone[34]. Their exact timing of formation and accretion, which is critical to reconstruct the origin and evolution of the dismembered OPS, was not known before.

Results

Four types of lithology are recognized in the study area: (1) massive to vesicular, aphyric to porphyritic lavas and primary volcanic breccias; (2) massive to volcaniclastic-bearing, shallow-marine carbonates; (3) red radiolarian cherts; and (4) well-bedded to boudinaged, fine-grained volcaniclastic turbidites. (1) to (3) appear as massive to lenticular, meter- to kilometer-sized blocks embedded in (4) (Fig. 2 and Supplementary Figs. 1 and 2). Among (1) to (3), an original depositional relationship is only observed locally between the volcanic rocks and the conformably overlying shallow-marine carbonates. This stratigraphic association is further highlighted by the occurrence of very well-rounded fragments of vesiculated basalts embedded in carbonate deposits (Supplementary Fig. 2), which suggest that the igneous rocks were locally subject to subaerial erosion before deposition in a shallow-marine environment.

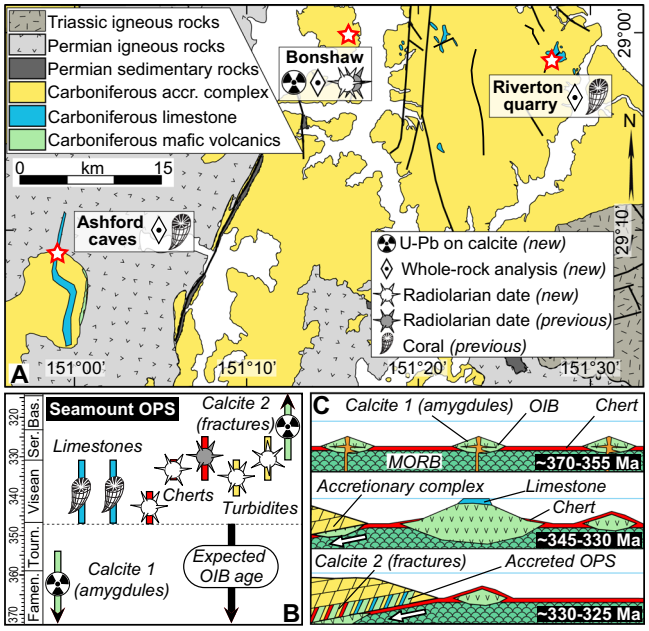

Fig. 2 Location, age, and tectonic interpretation of the sampled sections. **A** Geological map of the studied area (modified from ref. [35]). New data: calcite U-Pb ages, radiolarian ages (white fill; radiolarian plate in Supplementary Fig. 4), and whole-rock geochemistry. Previous ages: corals[34] and radiolarians[33] (gray fill). **B** Age constraints on the late Paleozoic seamount OPS. **C** Reconstruction of Panthalassan seamount OPS at its times of formation and accretion to Gondwana. Accr. Accretionary, Bas. Bashkirian, Famen. Famennian, MORB Mid-ocean ridge basalt, OIB Ocean island basalt, Ser. Serpukhovian.

Brittle deformation including orthogonal joints are visible among all the lithologies in the accretionary complex (Supplementary Figs. 2 and 3). Some joints in the volcanic rocks are filled with calcite and show a discrete shear component. The volcaniclastic turbidites are generally steeply-dipping and locally display slaty cleavage and vertical isoclinal folds, whereas the radiolarian cherts are characterized by open to tight folds.

Whole-rock geochemistry. The composition of volcanic and turbiditic rocks was determined by X-ray fluorescence (XRF), laser ablation–inductively coupled plasma–mass spectrometry (LA-ICP-MS), and four-acid digestion ICP-MS (see "Methods" and Supplementary Table 1). Because the samples are highly altered with common replacement of glass, feldspar and ferromagnesian phases by secondary clay minerals, their geochemical affinities are constrained here using the most immobile trace elements. Based on Nb/Y vs. Zr/Ti, the studied volcanic rocks are alkali basalt and trachyandesite (Fig. 3A). These rocks have an OIB-like signature in Nb/Yb vs. Th/Yb and primitive mantle-normalized trace element diagrams, including low contents in heavy rare earth elements, and a positive Nb–Ta anomaly (Fig. 3). In contrast, tuffaceous beds that form the bulk of the accretionary complex have supra-subduction affinities, with dacitic to rhyolitic compositions, prominent Nb–Ta and Ti negative anomalies in the multielement diagram, and high Th/Yb values for a given Nb/Yb ratio in a Nb/Yb vs. Th/Yb diagram.

In situ calcite geochronology and geochemistry. The age and fluid source of millimeter-sized calcite-filled amygdules of sample BNS19-01 and cross-cutting calcite-filled fractures of sample BNS19-02 from an OIB-like volcanic breccia were investigated by in situ LA-ICP-MS (see "Methods" and in ref. [36], Fig. 2,

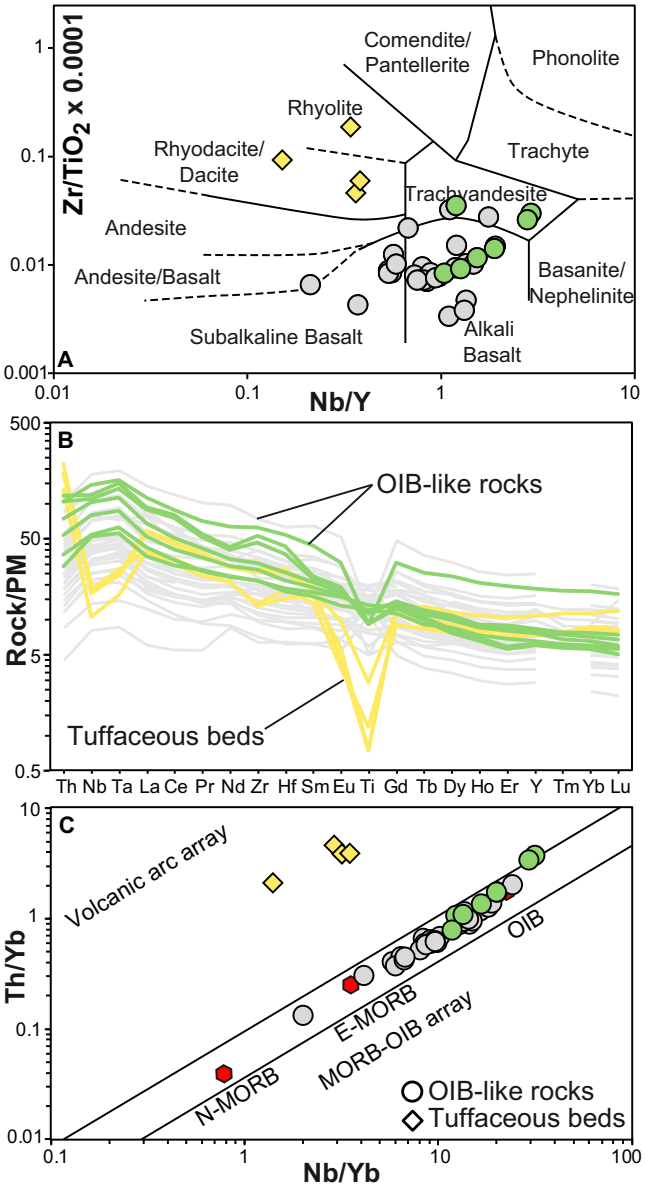

Fig. 3 Geochemistry of OIB-like rocks from the Texas Beds. Data: this study (yellow diamonds, green circles) and from ref. [35] (gray circles). Plots after: **A**[64], **C**[65]. **B** Primitive mantle (PM) after ref. [66]. **C** Average enriched mid-ocean ridge basalt (E-MORB), normal (N-MORB), and ocean island basalt (OIB) after ref. [67].

Supplementary Fig. 3, and Supplementary Tables 2 and 3). Calcite-filled amygdules from sample BNS19-01 provided an age of 366 ± 12 Ma (2σ, MSWD = 2.9, n = 23; Frasnian to early Tournaisian), whereas calcite-filled fractures from sample BNS19-02 yielded an age of 305 ± 26 Ma (2σ, MSWD = 2, n = 20; Fig. 4B, D; earliest Serpukhovian to early Kungurian). U and Pb concentrations in both samples are low, estimated to be ca. 150 ppb of U and ca. 40 ppb of Pb in BNS19-01, and ca. 10–20 ppb of U and ca. 10 ppb of Pb in BNS19-02. The relatively higher U-Pb contents in BNS 19-01 are reflected in a higher precision (3.2%) when compared to that of sample BNS 19-02 (8.5%). The lower precision of sample BNS19-02 may also be related to a relatively higher proportion of common Pb, which is indicated by analyses plotting toward high $^{207}Pb/^{206}Pb$ values. Despite the low U and Pb contents, the MSWD and 2σ precision values of the calcite phases are within the range of those of published LA-ICP-MS

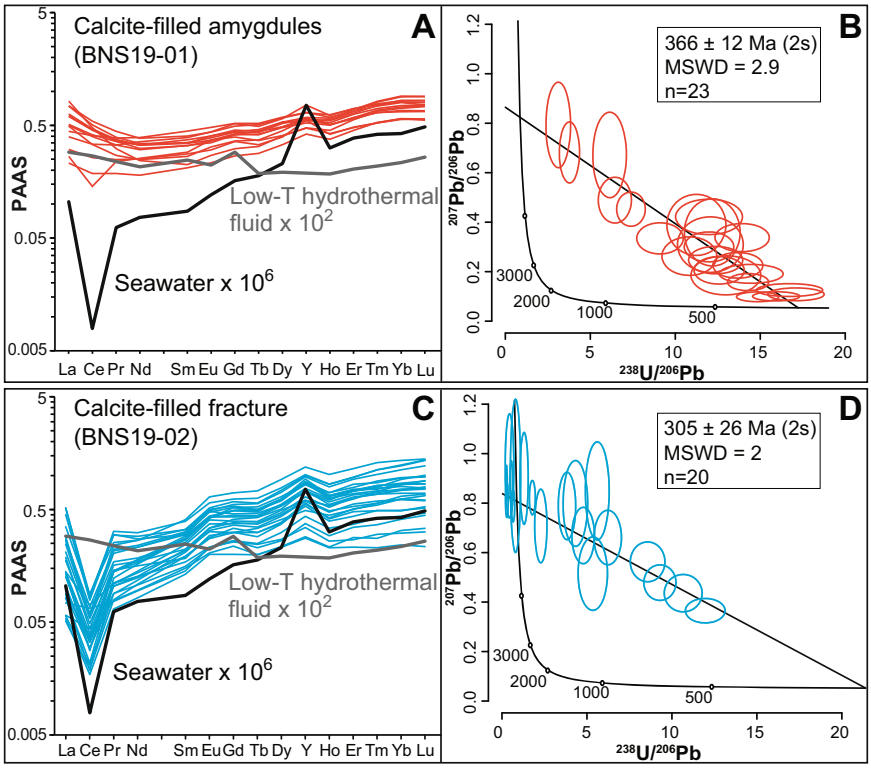

Fig. 4 Age and geochemistry of calcite-filled amygdules and fracture. A, **C** Shale-normalized REY patterns (rare earth elements and yttrium, REE + Y). Post-Archean Australian Shale (PAAS) after ref. [68], seawater after ref. [39], and low-temperature (low-T, <12 °C) hydrothermal fluid after ref. [38]. **B**, **D** Tera-Wasserburg concordia plots showing $^{238}U/^{206}Pb$ vs. $^{207}Pb/^{206}Pb$. MSWD mean squared weighted deviates.

U-Pb dates of carbonates[37]. Different ages of the amygdule-related and fracture-related calcites coincide with dissimilar shale-normalized trace element compositions. The former is consistent with precipitation from a low-temperature hydrothermal fluid mixed with seawater (i.e., <12 °C in ref. [38]), which is suggested by enrichments in light rare earth elements. In contrast, the calcites in fractures mimic the composition of the seawater[39], with prominent Ce and Y anomalies (Fig. 4A, C). Geochemical homogeneity of the two types of calcite suggests a simple precipitation history without post-precipitation contamination or dissolution/reprecipitation effects. These distinct ages and geochemical compositions are consistent with microscope petrographic observations that support two main generations of calcite in the basalts (i.e., in amygdules and veins; Supplementary Fig. 3).

Radiolarian biostratigraphy. Four radiolarian assemblages were determined in red cherts (1, 2) and yellowish volcaniclastic beds (3, 4) (Fig. 2B and Supplementary Fig. 4), the ages of which were determined using existing radiolarian biozonations[40–42]. The red cherts yield two distinct assemblages: (1) *Albaillella* sp. cf. *A. paradoxa* gr., *A. undulata*, and *A. indensis* (early to middle Visean, 347–339 Ma); (2) *A. cartalla, A. furcata, Scharfenbergia plenospongiosa*, and *Trilonche palimbola* (late Visean, 336–331 Ma). The yellowish tuffaceous beds present two different assemblages: (3) *Circulaforma anula*, *Entactinosphaera variabilis*, *Stigmosphaerostylus parva*, *S. variospina*, *S. unispina*, and *S. mirousi* (middle to late Visean, 340–331 Ma); (4) *A. cartalla*, *S. mirousi*, and *S. parva* (late Visean to late Serpukhovian, 336–325 Ma).

Discussion

Geological meaning of calcite U-Pb ages. The first generation of calcite formed in vesicles provides a new Late Devonian to earliest Carboniferous (ca. 378–354 Ma) minimal age of formation of the OIB-like volcanic breccia. This date is considered to be a good estimate of minimal formation age of the OIB because hydrothermal fluid circulation susceptible to precipitate calcite typically occurs < ca. 20 Myr after the formation of oceanic crust, e.g.[43,44]. Precipitation of calcite shortly after emplacement of the breccia in an oceanic intraplate setting is further supported by new and existing[33–35] younger biostratigraphic ages (≤ ca. 20 Myr; Fig. 2B) of adjacent blocks of open ocean sedimentary rocks and the matrix of the accretionary complex, which both record post-eruption sedimentation (Fig. 2B, C). The second generation of calcite formed in fractures during the Mid Carboniferous to early Permian (ca. 331–279 Ma), showing that brittle deformation occurred long after the formation of the volcanic breccia and its amygdule-related calcites. Precipitation of the second generation of calcite in a convergent margin setting is supported by the older biostratigraphic age on new radiolarian samples (≤ ca. 30 Myr; Fig. 2B) of the sedimentary matrix of the accretionary complex, which documents the age of accretion of the OPS (Fig. 2B, C). Remarkably, precipitation ages of the two generations of calcite are in very good agreement with the geochemical composition of the amygdules and veins (Fig. 4). Trace element data suggest that a more extensive hydrothermal fluid-rock interaction contributed to a more enriched composition of the amygdules when compared to that of subsequent fractures. This is expected, as mineral precipitation in isolated vesicles generally occurs during or shortly after the cooling of lava flows, whereas brittle deformation intervenes during later post-eruption stages[45]. Overall, data from U-Pb geochronology, biostratigraphy and calcite geochemistry suggest that U-Pb ages of the calcite in the amygdules provide geologically meaningful constraints on the formation age of the studied OIBs.

Constraints on oceanic island accretion to eastern Gondwana. The studied dismembered units are similar to other accreted

circum-Pacific oceanic islands that include OIB capped by shallow-marine carbonates and slope carbonate-bearing volcaniclastics[2,34]. Our data provide new information to reconstruct the original lithostratigraphy and geological history of this OPS (Fig. 4). Homogenous geochemical composition of the OIBs in the study area relative to that of other OIBs at the scale of the accretionary complex supports preservation of several volcanoes of similar ages that formed at a single intraplate hotspot. More specifically, the Late Devonian to earliest Carboniferous minimum age (ca. 378–354 Ma) of the OIBs estimated with our new U-Pb geochronology data from calcite-filled amygdules is slightly older than the Visean ages (ca. 347–331 Ma) of (1) the conformably overlying 500 m-thick shallow-marine carbonates (Ashford)[34], and (2) the chert blocks embedded in the same detrital matrix (Bonshaw). This suggests that the main volcanic phase of the island(s) had stopped by the Visean (ca. 347 Ma) to allow the formation of an atoll on the subsiding volcano, e.g.[34,46], with pelagic sedimentation on its deeper slopes. Substantial radiolarian pelagic deposition is not expected on the top of large seamounts due to current sweeping, but it could have occurred on the seamount slopes and in nearby oceanic basins[47], ultimately leading to their association with shallow-marine carbonate and OIB during accretion. This contrasts with the more common association of chert with MORB in other circum-Pacific accretionary complexes[2].

A maximum age of accretion of the OIBs is defined by the new late Visean to late Serpukhovian (ca. 335–325 Ma) biostratigraphic age of the enclosing tuffaceous turbidites, which deposited close to a volcanic arc ~30 Myr after the formation of the OIB (Fig. 2). Therefore, the younger, 305 ± 26 Ma age from calcite-filled fractures in the OIB is consistent with deformation after seamount accretion. Based on existing structural, geochronologic, and provenance data, brittle and ductile deformation of the Texas Beds is constrained to have happened before the onset of extension and oroclinal bending of the convergent margin at ca. 290 Ma[32,48,49]. Brittle deformation of the OIB in Bonshaw is thus broadly constrained to have occurred at the same time as the deformation of the Texas Beds, i.e., after oceanic island accretion and before oroclinal bending (between 330 and 290 Ma).

Taken together, our results show that U-Pb calcite geochronology on amygdules and veins yields important age constraints in dismembered altered OPS sequences, where direct dating of volcanic rocks is difficult to undertake with traditional geochronologic or biostratigraphic methods. Future applications may provide constraints on the subduction age vs. oceanic crust age of poorly dated Phanerozoic OPS, e.g.[50], whereas the study of well-preserved Precambrian OPS sequences may shed light on the evolution of old oceanic realms lacking fossils, e.g.[51]. The common occurrence of calcite-filled amygdules in volcanic rocks recovered in the oceans through dredging and drilling represents a future target for calcite U-Pb geochronology, as it can help unravel the age of oceanic crust formation. Provided that materials with adequate U-Pb contents are analyzed, it is expected that amygdule-related calcites would yield valuable age constraints in any Earth's tectonic setting associated with mafic magmatism or altered and weathered igneous rocks. Our results emphasize that REE + Y geochemistry combined with calcite U-Pb geochronology allows one to distinguish generations of calcite[52–54], which, in combination with other geological data, may help reconstruct meaningful sequences of eruption and deformation events in accretionary complexes.

Methods

Whole-rock geochemistry. Rock samples were crushed with a hammer into ~1–2 cm chips. Fresh chips were selected under a binocular microscope for geochemical analysis. For the volcaniclastic rocks, we analyzed carbonate-free, fine ash-rich beds (<0.0625 mm particles) because they are mostly composed of volcanic glass, the accumulation of which is expected to have took place shortly after eruption events due to its rapid chemical and mechanical weathering[55]. Although possibly biased toward the more silicic explosive volcanic products, the geochemistry of tuffaceous beds is otherwise expected to mimic that of coeval igneous rocks[56–58]. Coarser rocks such as sandstones were avoided because there are more likely to have incorporated a mixture of components from several sources, which could generate ambiguous geochemical signatures.

Major and trace element analysis of 2 igneous (BNS19-03A, BNS19-03B) and 3 volcaniclastic rocks (BNS19-04A, BNS19-04B, WRO19-02) were undertaken at Australian Laboratory Services Minerals Division, Brisbane, Australia. A prepared sample (1–5 g) is placed in a TGA furnace at ambient temperature, then heated to 105 °C and weighed, then heated to 1000 °C and weighed. The percent loss on ignition (LOI) is calculated from the difference in weight from 105 °C to 1000 °C divided by the weight at 105 °C. A prepared sample (0.66 g) is fused with a 12:22 lithium tetraborate–lithium metaborate flux which also includes an oxidizing agent (Lithium Nitrate), and then poured into a platinum mold. The resultant disk is in turn analyzed by XRF spectrometry. The XRF analysis is determined in conjunction with a loss-on-ignition at 1000 °C. The resulting data from both determinations are combined to produce a total. A prepared sample (0.100 g) is added to lithium metaborate/lithium tetraborate flux, mixed well and fused in a furnace at 1025 °C. The resulting melt is then cooled and dissolved in an acid mixture containing nitric, hydrochloric and hydrofluoric acids. This solution is then analyzed by ICP-MS. Standards, CGL 208, OREAS120, OREAS460, and OREAS100a, as well as two sample duplicates and one blank were analyzed.

Bulk rock samples R74681, R74685, R74686, R74687, DP09-001, and DP09-003 were reduced to powder at the Research School of Earth Sciences (RSES), Australian National University, using a pre-contaminated agate mill. The Environmental Laboratory at the Central Analytical Facility of the University of Stellenbosch determined major element contents by XRF and measured LOI. Trace element contents were measured by laser ablation–inductively coupled plasma source mass spectrometry (LA-ICP-MS) on tetraborate glasses at the RSES following procedures given in refs. [59,60]. Glass disks used for LA-ICP-MS analyses were prepared by fusion of 0.5000 g dried sample powder and 1.5000 g of "12–22" eutectic lithium metaborate–lithium tetraborate. A pulsed 193 nm ArF Excimer laser, with 50 mJ energy at a repetition rate of 5 Hz, coupled to an Agilent 7500S quadrupole ICP-MS were used. A synthetic glass (NIST612) was used as standard material. Four ablations with a 120 μm pit size were used to obtain the composition of each sample. Si values obtained from XRF analysis were used as internal standard. BCR-2 standard was additionally measured in each analytical series to check quality and consistency of the results.

Laser ablation ICP-MS U-Pb geochronologic and trace elemental analysis. Rock samples were processed at the School of Earth and Environmental Sciences, The University of Queensland. Samples were cut and mounted to round mounts with one-inch diameters. Samples mounts were polished with standard polishing procedures and finished with a 0.25 micrometer diamond suspension.

Laser ablation was achieved using an ASI RESOlution 193 ArF nm excimer laser system at the Radiogenic Isotope Facility of the Centre for Geoanalytical Mass Spectrometry. Following evacuation of air, He carrier gas was introduced into the laser cell at a flow rate of 0.35 l/min. 0.005 l/min of N_2 gas was also introduce to the laser cell to enhance the measurement sensitivity. The gas mixture was then introduced into the plasma torch of a Thermo iCAP RQ quadruple ICP-MS with 1.03 l/min Ar nebulizer gas. No reaction gas was employed. The laser was run with a 100-micronmetre diameter round spot at 10 Hz, with a measured instrument laser-fluence (laser pulse energy per unit area) of 2.5 J/cm^2. For U-Pb dating, each spot had 8 s of background, 20 s of data acquisition, and 15 s of wash out. For trace elemental analysis, each spot had 6 s of background, 25 s of data acquisition, and 10 s of wash out. Prior to data acquisition, ICP-MS signals were optimized during tuning. For our session, ~800 K cps of ^{238}U counts and ~0.23 of ^{206}Pb/^{238}U were achieved for measuring NIST612 glass using line scans of 3 um/s, 10 Hz, 50 um round laser pit, and 3 J/cm^2.

Our samples have very low U and Pb (several ppb) and many spots were not measurable by a single-collector ICP-MS. We measured >200 spots across each sample but only recovered ~10–30 data points. U-Pb isotopes for geochronology (^{206}Pb, ^{207}Pb, ^{208}Pb, ^{232}Th, and ^{238}U) were measured with the following dwell times, ^{206}Pb (0.025 s), ^{207}Pb (0.055 s), ^{208}Pb (0.005), ^{232}Th (0.005 s), and ^{238}U (0.02 s). Both glass standard NIST614 and matrix-matched calcite standards were measured, bracketing unknown spots. NIST614 glass was used for correction of ^{207}Pb/^{206}Pb fractionation and instrument drift in the ^{238}U/^{206}Pb ratio[61]. Raw data were processed using Iolite software v3.64[62]. After the initial correction, a matrix-matched calcite reference material of known age was used for further correction of matrix-related mass bias impacting the measured ^{238}U/^{206}Pb ratios, following the approach described elsewhere, as summarized in[36]. We used our in-house calcite reference materials (PTKD and AHX-1D[36]) and one international reference material WC-1[63] in our analytical sessions. The international reference material, WC-1, was used as a monitoring standard to check data accuracy, which yielded 251.2 ± 1.9 Ma (2σ), consistent with the recommended value (254.4 ± 6.4 Ma, 2σ)[63].

Trace elemental analysis was conducted in the same ablation areas as the U-Pb spots but without overlapping with U-Pb spots. Standard material NIST612 was used.

^{43}Ca was measured as an internal standard. Data reduction was conducted using the Iolite software v3.64[62] with the Trace Element data reduction scheme. All reported concentrations were after international standardization using Ca (Ca = 40.1%).

Data availability

All datasets generated during this study have been archived in Zenodo and can be accessed from this link: https://doi.org/10.5281/zenodo.6393844.

Received: 18 August 2021; Accepted: 25 April 2022;
Published online: 12 May 2022

References

1. Isozaki, Y., Maruyama, S. & Furuoka, F. Accreted oceanic materials in Japan. *Tectonophysics* **181**, 179–205 (1990).
2. Safonova, I. et al. Recognizing OIB and MORB in accretionary complexes: a new approach based on ocean plate stratigraphy, petrology and geochemistry. *Gondwana Res.* **33**, 92–114 (2016).
3. Hofmann, A. Mantle geochemistry: the message from oceanic volcanism. *Nature* **385**, 219–229 (1997).
4. Regelous, M., Hofmann, A. W., Abouchami, W. & Galer, S. J. G. Geochemistry of lavas from the Emperor Seamounts, and the geochemical evolution of Hawaiian magmatism from 85 to 42 Ma. *J. Petrol.* **44**, 113–140 (2003).
5. Torsvik, T. H. et al. Pacific-Panthalassic reconstructions: overview, errata and the way forward. *Geochem. Geophys. Geosyst.* **20**, 3659–3689 (2019).
6. Cawood, P. A. et al. Accretionary orogens through Earth history. *Geol. Soc. Spec. Publ.* **318**, 1–36 (2009).
7. Nokleberg, W. J. et al. Phanerozoic tectonic evolution of the Circum-North Pacific. USGS Professional Paper 1626, 122 (2000).
8. Mortimer, N. New Zealand's geological foundations. *Gondwana Res.* **7**, 261–272 (2004).
9. Hall, R. Late Jurassic–Cenozoic reconstructions of the Indonesian region and the Indian Ocean. *Tectonophysics* **570–571**, 1–41 (2012).
10. Spikings, R. et al. The geological history of northwestern South America: from Pangaea to the early collision of the Caribbean large igneous province (290–75 Ma). *Gondwana Res.* **27**, 95–139 (2015).
11. Campbell, M. J., Rosenbaum, G., Allen, C. M. & Spandler, C. Continental crustal growth processes revealed by detrital zircon petrochronology: Insights from Zealandia. *J. Geophys. Res. Solid Earth* **125**, e2019JB019075 (2020).
12. Wakita, K., Nakagawa, T., Sakata, M., Tanaka, N. & Oyama, N. Phanerozoic accretionary history of Japan and the western Pacific margin. *Geol. Mag.* **158**, 13–29 (2021).
13. Hagstrum, J. T. & Murchey, B. L. Deposition of Franciscan Complex cherts along the paleoequator and accretion to the American marginal tropical paleolatitudes. *Geol. Soc. Am. Bull.* **105**, 766–778 (1993).
14. Ando, A., Kodama, K. & Kojima, S. Low-latitude and Southern Hemisphere origin of Anisian (Triassic) bedded chert in the Inuyama area, Mino terrane, central Japan. *J. Geophys. Res.* **106**, 1973–1986 (2001).
15. Bill, M., O'Dogherty, L., Guex, J., Baumgartner, P. O. & Masson, H. Radiolarite ages in Alpine-Mediterranean ophiolites: constraints on the oceanic spreading and the Tethys-Atlantic connection. *Bull. Geol. Soc. Am.* **113**, 129–143 (2001).
16. Spörli, K. B., Aita, Y., Hori, R. S. & Takemura, A. Results of multidisciplinary studies of the Permian/Triassic ocean floor sequence (Waipapa Terrane) at Arrow Rocks, Northland, New Zealand. *GNS Sci. Monogr.* **24**, 219–229 (2007).
17. Safonova, I. & Santosh, M. Accretionary complexes in the Asia-Pacific region: tracing archives of ocean plate stratigraphy and tracking mantle plumes. *Gondwana Res.* **25**, 126–158 (2014).
18. Reuber, I., Colchen, M. & Mevel, C. The geodynamic evolution of the South-Tethyan, margin in Zanskar, NW-Himalaya, as revealed by the Spongtang ophiolitic melanges. *Geodin. Acta* **1**, 283–296 (1987).
19. Sano, H. Impact of long-term climate change and sea-level fluctuation on Mississippian to Permian mid-oceanic atoll sedimentation (Akiyoshi Limestone Group, Japan). *Palaeogeogr. Palaeoclimatol. Palaeoecol.* **236**, 169–189 (2006).
20. Verati, C. & Jourdan, F. Modelling effect of sericitization of plagioclase on the 40K/40Ar and 40Ar/39Ar chronometers: Implication for dating basaltic rocks and mineral deposits. *Geol. Soc. Spec. Publ.* **378**, 155–174 (2014).
21. Eggleton, R. A., Foudoulis, C. & Varkevisser, D. Weathering of basalt: changes in rock chemistry and mineralogy. *Clays Clay Miner.* **35**, 161–169 (1987).
22. Niu, Y. & O'Hara, M. J. Origin of ocean island basalts: a new perspective from petrology, geochemistry, and mineral physics considerations. *J. Geophys. Res.* **108**, 1–19 (2003).
23. Staudigel, H. *Treatise on Geochemistry Ch. 3.15* (Pergamon, 2003).
24. Boehnke, P., Watson, E. B., Trail, D., Harrison, T. M. & Schmitt, A. K. Zircon saturation re-revisited. *Chem. Geol.* **351**, 324–334 (2013).
25. Ware, B. & Jourdan, F. 40Ar/39Ar geochronology of terrestrial pyroxene. *Geochim. Cosmochim. Acta* **230**, 112–136 (2018).
26. Olgers, F., Flood, P. G. & Robertson, A. D. *Palaeozoic Geology of the Warwick and Goondiwindi 1:250,000 Sheet Areas, Queensland and New South Wales* 109 (Australian Bureau of Mineral Resources Report 164, 1974).
27. Korsch, R. J. & Harrington, H. J. Oroclinal bending, fragmentation and deformation of Terranes in the New England Orogen, Eastern Australia. In *Terrane Accretion and Orogenic Belts* (eds Leitch E.C. and Scheibner E.) Vol. 19, 129–139 (1987).
28. Glen, R. A. The Tasmanides of eastern Australia. *Geol. Soc. Spec. Publ.* **246**, 23–96 (2005).
29. Leitch, E. C. Plate tectonic interpretation of the Paleozoic history of the New England fold belt. *Geol. Soc. Am. Bull.* **86**, 141–144 (1975).
30. Murray, C. G., Ferguson, C. L., Flood, P. G., Whitaker, W. G. & Korsch, R. J. Plate tectonic model for the Carboniferous evolution of the New England Fold Belt. *Aust. J. Earth Sci.* **34**, 213–236 (1987).
31. Rosenbaum, G., Li, P. & Rubatto, D. The contorted New England orogen (eastern Australia): new evidence from U-Pb geochronology of Early Permian granitoids. *Tectonics* **31**, TC1006 (2012).
32. Li, P., Rosenbaum, G. & Vasconcelos, P. Chronological constraints on the Permian geodynamic evolution of eastern Australia. *Tectonophysics* **617**, 20–30 (2014).
33. Aitchison, J. C., Flood, P. G. & Spiller, F. C. P. Tectonic setting and paleoenvironment of terranes in the southern New England orogen, eastern Australia as constrained by radiolarian biostratigraphy. *Palaeogeogr. Palaeoclimatol. Palaeoecol.* **94**, 31–54 (1992).
34. Flood, P. G. Exotic seamounts within Gondwanan accretionary complexes, Eastern Australia. *NEO '99 Conference at the University of New England, Armidale*, 23–29 (1999).
35. Donchak, P. J. T., Bultitude, R. J., Purdy, D. J. & Denaro, T. J. *Geology and Mineralisation of the Texas Region, South-Eastern Queensland*. Queensland Geology 11, 95 (2007).
36. Yang, P. et al. In situ LA-ICPMS U-Pb dating and geochemical characterization of fault-zone calcite in the central Tarim Basin, northwest China: Implications for fluid circulation and fault reactivation. *Chem. Geol.* **568**, 120125 (2021).
37. Roberts, N. M. W. et al. Laser ablation inductively coupled plasma mass spectrometry (LA-ICP-MS) U–Pb carbonate geochronology: strategies, progress, and limitations. *Geochronology* **2**, 33–61 (2020).
38. Zeng, Z. et al. Factors affecting the rare earth element compositions in massive sulfides from deep-sea hydrothermal systems. *Geochem. Geophys. Geosyst.* **16**, 2679–2693 (2015).
39. Zhang, J. & Nozaki, Y. Rare earth elements and yttrium in seawater: ICP-MS determinations in the East Caroline, Coral Sea, and South Fiji basins of the western South Pacific Ocean. *Geochim. Cosmochim. Acta* **60**, 4631–4644 (1996).
40. Wonganan, N., Randon, C. & Caridroit, M. Mississippian (early Carboniferous) radiolarian biostratigraphy of northern Thailand (Chiang Dao area). *Geobios* **40**, 875–888 (2007).
41. Won, M.-Z. & Seo, E.-H. Lower Carboniferous radiolarian biozones and faunas from Bergishes Land, Germany. *J. Palaeontol. Soc. Korea* **26**, 193–269 (2010).
42. Aitchison, J. C., Suzuki, N., Caridroit, M., Danelian, T. & Noble, P. Paleozoic radiolarian biostratigraphy. *Geodiversitas* **39**, 503–531 (2017).
43. Coogan, L. A., Parrish, R. R. & Roberts, N. M. Early hydrothermal carbon uptake by the upper oceanic crust: Insight from in situ U-Pb dating. *Geology* **44**, 147–150 (2016).
44. Quandt, D. et al. Geochemistry of vein calcites hosted in the Troodos Pillow Lavas and their implications for the timing and physicochemical environment of fracturing, fluid circulation, and vein mineral growth. *Geochem. Geophys. Geosyst.* **20**, 5913–5938 (2019).
45. Neuhoff, P. S., Fridriksson, T., Arnorsson, S. & Bird, D. K. Porosity evolution and mineral paragenesis during low-grade metamorphism of basaltic lavas at Teigarhorn, Eastern Iceland. *Am. J. Sci.* **299**, 467–501 (1999).
46. Staudigel, H. & Clague, D. A. The geological history of deep-sea volcanoes. *Oceanography* **23**, 58–71 (2010).
47. Baumgartner, P. O. Mesozoic radiolarites—accumulation as a function of sea surface fertility on Tethyan margins and in ocean basins. *Sedimentology* **60**, 292–318 (2013).
48. Li, P., Rosenbaum, G. & Donchak, P. J. T. Structural evolution of the Texas orocline, eastern Australia. *Gondwana Res.* **22**, 279–289 (2012).
49. Shaanan, U., Rosenbaum, G. & Wormald, R. Provenance of the Early Permian Nambucca block (eastern Australia) and implications for the role of trench retreat in accretionary orogens. *Geol. Soc. Am. Bull.* **127**, 1052–1063 (2015).
50. Wakabayashi, J. Structural context and variation of ocean plate stratigraphy, Franciscan Complex, California: insight into melange origins and subduction accretion processes. *Prog. Earth Planet. Sci.* **4**, 18 (2017).

51. Kusky, T. et al. Recognition of ocean plate stratigraphy in accretionary orogens through Earth history: a record of 3.8 billion years of sea floor spreading, subduction, and accretion. *Gondwana Res.* **24**, 501–547 (2013).
52. Peyrotty, G., Brigaud, B. & Martini, R. δ18O, δ13C, trace elements and REE in situ measurements coupled with U–Pb ages to reconstruct the diagenesis of upper Triassic atoll-type carbonates from the Panthalassa Ocea. *Mar. Pet. Geol.* **120**, 104520 (2020).
53. Celestino, M. A. L. et al. Structural control and geochronology of Cretaceous carbonate breccia pipes, Crato Formation, Araripe Basin, NE Brazil. *Mar. Pet. Geol.* **132**, 105190 (2021).
54. Simpson, A. et al. In-situ calcite U-Pb geochronology of hydrothermal veins in Thailand: New constraints on Indosinian and Cenozoic deformation. *J. Asian Earth Sci.* **206**, 104649 (2021).
55. Schacht, U., Wallmann, K., Kutterolf, S. & Schmidt, M. Volcanogenic sediment—seawater interactions and the geochemistry of pore waters. *Chem. Geol.* **249**, 321–338 (2008).
56. Clift, P. D., Degnan, P. J., Hannigan, R. & Blusztajn, J. Sedimentary and geochemical evolution of the Dras forearc basin, Indus suture, Ladakh Himalaya, India. *Geol. Soc. Am. Bull.* **112**, 450–466 (2000).
57. Robertson, A. H. F. et al. Depositional setting, provenance, and tectonic-volcanic setting of Eocene-Recent deep-sea sediments of the oceanic Izu-Bonin forearc, northwest Pacific (IODP Expedition 352). *Int. Geol. Rev.* **60**, 1816–1854 (2018).
58. Schindlbeck, J. C. et al. One million years tephra record at IODP Sites U1436 and U1437: insights into explosive volcanism from the Japan and Izu arcs. *Isl. Arc* **27**, e12244 (2018).
59. Eggins, M. S. Laser ablation ICP-MS analysis of geological materials prepared as lithium borate glasses. *Geostand. Geoanalytical Res.* **27**, 147–162 (2003).
60. Longerich, H. P., Jackson, S. E. & Gunther, D. Laser ablation inductively coupled plasma mass spectrometric transient signal data acquisition and analyte concentration calculation. *J. Anal. At. Spectrom.* **11**, 899–904 (1996).
61. Woodhead, J. D. & Hergt, J. M. Strontium, neodymium and lead isotope analyses of NIST glass certified reference materials: SRM 610, 612, 614. *Geostand. Newslett.* **25**, 261–266 (2007).
62. Paton, C., Hellstrom, J., Paul, B., Woodhead, J. & Hergt, J. Iolite: freeware for the visualisation and processing of mass spectrometric data. *J. Anal. At. Spectrom.* **26**, 2508–2518 (2011).
63. Roberts, N. M. et al. A calcite reference material for LA-ICP-MS U-Pb geochronology. *Geochem. Geophys. Geosyst.* **18**, 2807–2814 (2017).
64. Winchester, J. A. & Floyd, P. A. Geochemical discrimination of different magma series and their differentiation products using immobile elements. *Chem. Geology* **20**, 325–343 (1977).
65. Pearce, J. A. Geochemical fingerprinting of oceanic basalts with applications to ophiolite classification and the search for Archean oceanic crust. *Lithos* **100**, 14–48 (2008).
66. McDonough, W. F. & Sun, S. S. The composition of the Earth. *Chem. Geol.* **120**, 223–253 (1995).
67. Sun, S. S. & McDonough, W. F. Chemical and isotopic systematics of oceanic basalts: implications for mantle composition and processes. *Geol. Soc. Spec. Publ.* **42**, 313–345 (1989).
68. McLennan, S. M. Rare earth elements in sedimentary rocks: influence of provenance and sedimentary processes. Geochemistry and mineralogy of rare earth elements. *Rev. Mineral.* **21**, 169–200 (1989).

Acknowledgements
G.A. is supported by a postdoctoral fellowship of the Swiss National Science Foundation (grant no. 178098) and the Robert Day Postdoctoral Fellowship in Palaeontology and Stratigraphy of the University of Queensland. R.Z. is supported by a UQ ECR grant. Thanks to Peter Flood for introducing us to the studied area and for sharing samples. We thank Derya Guerer for the help in the field. No sampling permission was required to collect the rocks used in this study.

Author contributions
G.A. and R.Z. designed the project with input from D.M.B. and J.C.A. G.A. wrote the manuscript with contributions from all co-authors. G.A. and D.M.B. conducted fieldwork. G.A., R.Z., D.M.B., and J.Z. performed the analysis. All the authors contributed to the interpretation of the results.

Competing interests
The authors declare no competing interests.

Additional information
Supplementary information The online version contains supplementary material available at https://doi.org/10.1038/s43247-022-00446-1.

Correspondence and requests for materials should be addressed to Goran Andjić or Renjie Zhou.

Peer review information *Communications Earth & Environment* thanks Nick Roberts, Randall Parrish and the other, anonymous, reviewer(s) for their contribution to the peer review of this work. Primary Handling Editors: João Duarte, Joe Aslin, Heike Langenberg.